Immunobiology 218 (2013) 496–505

Contents lists available at SciVerse ScienceDirect

Immunobiology

journal homepage: www.elsevier.com/locate/imbio

New analogs of the clinical complement inhibitor compstatin with subnanomolar affinity and enhanced pharmacokinetic properties

Hongchang Qu[a,1,2], Daniel Ricklin[a,1], Hongjun Bai[a], Hui Chen[a], Edimara S. Reis[a], Mateusz Maciejewski[b], Apostolia Tzekou[a], Robert A. DeAngelis[a], Ranillo R.G. Resuello[c], Florea Lupu[d], Paul N. Barlow[b], John D. Lambris[a,*]

[a] Department of Pathology and Laboratory Medicine, University of Pennsylvania, Philadelphia, USA
[b] School of Chemistry and School of Biological Sciences, University of Edinburgh, United Kingdom
[c] Simian Conservation Breeding and Research Center (SICONBREC), Philippines
[d] Cardiovascular Biology Research Program, Oklahoma Medical Research Foundation, USA

ARTICLE INFO

Article history:
Received 12 June 2012
Accepted 12 June 2012

Keywords:
Complement
Innate immunity
Compstatin
Inhibitor
Peptide therapeutic
Pharmacokinetics

ABSTRACT

Therapeutic modulation of the complement system has become increasingly important in line with the growing recognition of the role of complement in numerous diseases. Compstatin, a peptidic inhibitor that acts at the central level of the complement cascade, is currently in clinical evaluation but routes to improve its efficacy have not yet been fully explored. Here, we report improvements in both the inhibitory potency and pharmacokinetic parameters of compstatin that broaden its clinical applications. Selective modification of the compstatin N-terminus with non-proteinogenic amino acids resulted in the first analogue with subnanomolar binding affinity (K_D = 0.5 nM) and other similarly potent derivatives with improved solubility in clinically relevant solvents. Detailed structure–activity relationship studies based on biophysical and computational methods revealed key structural determinants for the observed improvements. Importantly, pharmacokinetic evaluation in non-human primates revealed target-driven elimination kinetics with plasma half-life values exceeding expectations for peptidic drugs (close to 12 h). This successful optimization strategy is expected to pave the way for systemic administration of compstatin in a range of clinical conditions.

Introduction

The involvement of the complement system in various inflammatory, autoimmune and neurodegenerative diseases, as well as cancer, sepsis, transplant rejection and biomaterial-related complications, has rendered it an attractive target for pharmaceutical intervention (Lachmann and Smith 2009; Markiewski and Lambris 2007; Ricklin et al. 2010; Ricklin and Lambris 2007). In recent years, there has been a surge in the development of therapeutic complement inhibitors ranging from small molecules to biopharmaceuticals. These efforts have already resulted in the approval of human C1-inhibitor (*e.g.*, Cinryze, ViroPharma) for hereditary angioedema, and a C5 antibody (Eculizumab; Soliris, Alexion Pharmaceuticals) for paroxysmal nocturnal hemoglobinuria (PNH) and atypical hemolytic uremic syndrome. However, a multitude of targets within the complement cascade and the desirability of pathway-specific inhibitors, together with the high treatment costs associated with both Soliris and Cinryze, are driving strong demand for alternatives. Other complement inhibitors currently in (pre-) clinical evaluation include soluble complement receptor 1 (TP10/CDX-1135, Celldex), targeted regulator constructs (*e.g.*, TT30, Alexion), the C5a receptor antagonist PMX53, and analogues of the C3-binding peptide compstatin (Emlen et al. 2010; Qu et al. 2009c; Ricklin and Lambris 2007; Wagner and Frank 2010).

Derivatives of compstatin, a 13-residue cyclic peptide that inhibits the activation of the central complement component C3 (Fig. 1), have significant potential for clinical applications (Ricklin and Lambris 2008). Recent examples include the reduction of filter-induced adverse effects during hemodialysis and organ preservation in sepsis (Kourtzelis et al. 2010; Silasi-Mansat et al. 2010). Notably, the intravitreal use of compstatin analogs has

Abbreviations: AMD, age-related macular degeneration; C3, complement component 3; DPBS, Dulbecco's phosphate-buffered saline; HDMS, high definition mass spectrometry; NHP, non-human primate; NMR, nuclear magnetic resonance; PNH, paroxysmal nocturnal hemoglobinuria; Sar, sarcosine; SPE, solid-phase extraction; SPR, surface plasmon resonance; UPLC, ultra performance liquid chromatography; WFI, water for injection.

☆ The solution structure of compstatin analog Cp10 has been deposited at the BMRB database (www.bmrb.wisc.edu) with accession number 21018.

* Corresponding author. Tel.: +1 215 746 5765.
E-mail address: lambris@upenn.edu (J.D. Lambris).

[1] These authors contributed equally.

[2] Present address: PolyPeptide Laboratories Inc. 365 Maple Avenue, Torrance, CA 90503, USA.

0171-2985/$ – see front matter © 2012 Elsevier GmbH. All rights reserved.
http://dx.doi.org/10.1016/j.imbio.2012.06.003

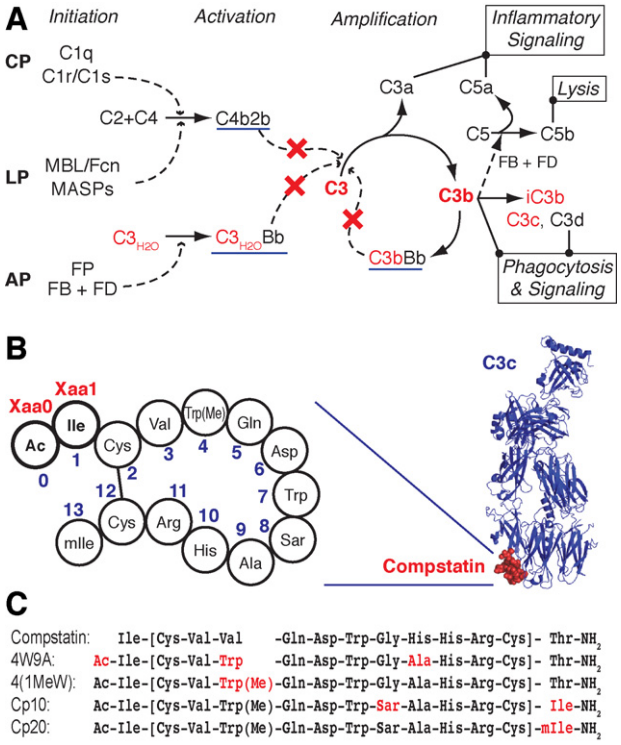

Fig. 1. Targets and structure of compstatin. (A) Simplified schematic representation of the human complement system showing initiation *via* the classical (CP), lectin (LP) or alternative (AP) pathway, amplification *via* C3/C3b and effector functions. C3 convertase complexes are underlined in blue. Complement inhibition by compstatin analogs is indicated by cross marks, and binding targets are highlighted in red. (B) Binding site of compstatin in the co-crystal structure with C3c (right; PDB 2QKI) and schematic view of the cyclic peptide sequence of compstatin analog Cp20. The traditional numbering scheme is shown in blue, and positions changed in this study (Xaa0, Xaa1) are indicated in red. (C) Peptide sequences of previous lead compounds, which are used as standards and references in this study. Residues that have been improved between each optimization cycle are marked in red. Analog 4(1MeW) has also been designated as POT-4 and AL-78898A in ongoing clinical trials. (For interpretation of the references to colour in this figure legend, the reader is referred to the web version of the article.)

shown promising results in the treatment of age-related macular degeneration (AMD), both in non-human primate (NHP) studies and in phase I clinical trials (Chi et al. 2010; Deal Watch 2009). One compstatin analog (4(1MeW), Fig. 1C; POT-4, Potentia; AL-78898A, Alcon) is currently being evaluated in a phase II clinical trial for exudative AMD (Alcon Research). The low molecular weight of compstatin, its high specificity and efficacy, and its ability to simultaneously inhibit all complement activation and amplification pathways contribute to a beneficial drug profile (Qu et al. 2009c; Ricklin and Lambris 2007, 2008). Extended clinical applications (*e.g.*, systemic administration), however, place additional demands on the molecular properties of compstatin derivatives.

In our previous optimization efforts, we successfully employed a variety of strategies for improving the potency (Qu et al. 2011), stability (Knerr et al. 2011) or pharmacokinetic profile of compstatin (Qu et al. 2009a,b). Recently, we disclosed a new series of compstatin analogs with significantly improved binding affinity and inhibitory potency as a result of backbone N-methylation and C-terminal substitution (Kourtzelis et al. 2010; Qu et al. 2011). Based on thermodynamic and kinetic data, we hypothesized that the positive effect of N-methylation within the cyclic core of the peptide structure arises from the predominance in solution of conformers that mimic the compact bound form of the peptide. Here, we report that we were able to support that hypothesis by solving, by NMR, the solution structure of the recently disclosed compstatin analog Cp10 (Fig. 1C), which carries an N-methyl group at position 8 (Qu et al. 2011). At the same time, we screened various modifications of the N-terminus of the current lead compound, Cp20 (Fig. 1C) (Qu et al. 2011), in order to further improve its properties. We thus identified several analogs with large gains in binding affinity and inhibitory potency, as well as improved solubility and highly favorable plasma half-life. These findings are expected to directly benefit the use of compstatin in a variety of disease models and clinical applications.

Materials and methods

Reagents and proteins

Rink amide MBHA resin, Oxyma (ethyl 2-cyano-2-[hydroxyimino]acetate) and the following Fmoc-amino acids were obtained from Novabiochem (San Diego, CA): Ile, Cys(Trt), Val, Tyr(tBu), Gln(Trt), Asp(OtBu), Trp(Boc), Gly, Sar, Ala, MeAla, His(Trt), Arg(Pbf), MeIle, Phe, MePhe and DCha. DIC and Fmoc-Trp(Me)-OH were purchased from AnaSpec (San Jose, CA). NMP and DCM were obtained from Fisher Scientific (Pittsburgh, PA). All other chemical reagents for synthesis were purchased from Sigma-Aldrich (St. Louis, MO) and used without further purification. Human C3b was generated from plasma-purified C3 by limited trypsinization and site-specifically biotinylated at its thioester moiety using biotin-maleimide as described before (Magotti et al. 2009; Qu et al. 2011). For NHP specificity experiments, C3 was purified from the plasma of cynomolgus and rhesus monkeys (both from Alpha Genesis Inc., Yemassee, SC) and baboons (collected at the University of Oklahoma Health Science Center animal facility) as described for human C3.

Peptide synthesis

All peptides were synthesized manually by Fmoc solid-phase methodology using DIC and Oxyma as coupling reagents. For the synthesis of the linear peptides, rink amide MBHA resin (0.59 mmol/g) was placed into a glass reaction vessel equipped with frits on the bottom and swollen in DCM for 30 min. After removal of the Fmoc protecting group (25% piperidine in NMP, 5 and 10 min), the resin was washed 7 times with NMP and twice with DCM, and the individual amino acids were coupled to the resin. For each coupling, 3 equiv. of the amino acid, Oxyma, and DIC were used, with 10 min preactivation in NMP. All couplings were performed for 1 h and monitored by either Kaiser test or chloranil test. In the case of a positive test result, the coupling was repeated until a negative test result was observed. The synthesis was stopped after the coupling of the second Cys(Trt). Then the resin was split in polypropylene syringes with frits on the bottom (Torviq, Niles, MI) and additional amino acids were coupled as needed for each analog.

Upon completion of the solid phase synthesis, the resin was washed four times each with NMP, DCM, and DCM/diethylether (1:1), and dried under high vacuum for 4 h. The peptides were cleaved from the resin with a mixture of 94% TFA, 2.5% water, 2.5% EDT and 1% TIPS for 2 h. After evaporation of the TFA under vacuum, the peptides were precipitated and washed three times with ice-cold diethyl ether. The liquid was separated from the solid by centrifugation and decanted. The crude peptides were dried in a vacuum and dissolved to 1 mg/mL in 30% acetonitrile with 0.1% TFA. The pH of the solution was adjusted to 7–8 using concentrated ammonium hydroxide. Dilute hydrogen peroxide (1:100, 2 equiv.) was added to the solution under vigorous stirring. Cyclization was monitored by MALDI-TOF mass spectrometry (MS). Once the reaction was completed, TFA was added to lower the pH to 2, and the solution was lyophilized. The crude peptide was purified using

RP-HPLC as described previously (Qu et al. 2011). The resulting TFA salt form of each peptide was converted to the acetate salt form using anion exchange resin in sodium acetate buffer (Roux et al. 2008). The purified peptides were >95% pure as determined by analytical RP-HPLC (Luna C_{18}, 5 μm 100 Å column, 250 mm × 4.60 mm; Phenomenex, Torrance, CA). The mass of each peptide was confirmed using a MALDI micro MX instrument (Waters, Milford, MA) or a SYNAPT G2-S high definition mass spectrometry (HDMS) instrument (Waters).

Elucidation of solution structures

The solution structure of compstatin analog Cp10 was elucidated using comprehensive nuclear magnetic resonance (NMR) analysis by recording DQF-COSY, TOCSY, and NOESY spectra at 15 °C and pH 6.0. The structures were calculated using Xplor-NIH software involving CHARMM19 and CHARMM20 force fields. In addition, molecular dynamics (MD) simulations between analogs 4W9A and Cp20 (derivative with Trp instead of Trp[Me] at position 4) were performed to further investigate the impact of N-methylation at position 8 on the solution structure. Detailed method descriptions for both NMR and MD analyses are provided in Supplementary Methods.

Complement inhibition assays

The ability of the compstatin analogs to inhibit complement activation initiated *via* the classical pathway was assessed by ELISA as described elsewhere (Katragadda et al. 2006; Mallik et al. 2005). The percent inhibition was plotted against the peptide concentration, and the resulting data set was fitted to the logistic dose-response function using Origin 8.0 software. IC_{50} values were obtained from the fitted parameters that produced the lowest χ^2 value. Each analog was assayed at least three times.

Binding studies

The binding affinity and kinetic profiles of the compstatin analogs with C3b was characterized using surface plasmon resonance (SPR) using a Biacore 3000 instrument (GE Healthcare, Corp., Piscataway, NJ). Data were recorded at 25 °C using PBS-T (10 mM sodium phosphate, 150 mM NaCl, 0.005% Tween-20, pH 7.4) as running buffer. Biotinylated C3b was captured on two flow cells of a streptavidin sensor chip (GE Healthcare) at densities of about 3000 and 5000 resonance units (RU); untreated flow cells were used as a reference surface. A single cycle approach was used for kinetic analysis; sets of five increasing concentrations of each compound (0.5–40 nM) were injected over the chip surface consecutively in a single cycle without regeneration at a flow rate of 30 μL/min. Individual injections within a cycle were 2 min long with a 5-min dissociation between injections. After the end of the last injection, a 40-min dissociation time was allowed. Analog 4(1MeW) (Katragadda et al. 2006) was included in each experimental series as an internal control. Data were processed in Scrubber (v2.0c; BioLogic Software, Campbell, Australia); the signals from an untreated flow cell and an ensemble of buffer blank injections were subtracted to correct for buffer effects and injection artifacts. The kinetic evaluation was performed in BiaEvaluation using a single cycle kinetic template (kindly provided by GE Healthcare) by globally fitting each data set to a 1:1 Langmuir binding model to achieve association and dissociation rates (k_a and k_d, respectively); the equilibrium dissociation constant (K_D) was calculated from the equation $K_D = k_d/k_a$. Each assay was performed at least twice. For superimposition of binding curves, the SPR signal of each peptide was divided by the corresponding molecular weight and multiplied by the average mass of all compounds in the data set.

For the NHP specificity experiments, C3 from human, cynomolgus monkey, rhesus monkey, and baboon plasma was immobilized on individual flow cells of CM5 sensor chips (GE Healthcare) using standard amine coupling to reach target densities of 6000–7000 RU. Peptides Cp20, 3 and 14 were quantitatively evaluated using a single cycle kinetic approach as described above. To visually compare the kinetic profiles independently of differences in target density or activity, each binding curve was normalized to the maximum response and superimposed in Origin.

Computational analysis

Docking studies were performed to compare computational with experimental free energy values for all tested analogs, in order to arrive at models for explaining and predicting effects of N-terminal compstatin modification. A detailed description of these methods can be found in Supplementary Methods.

Solubility studies

Approximately 5 mg of each peptide (acetate form) was weighted out into separate LoBind Eppendorf tubes and 50 μL water for injection (WFI) was added to each tube. Each sample was centrifuged at 13,000 rpm for 2 min and diluted for measuring the optical density (OD) at 280 nm using a NanoDrop 2000 spectrophotometer (ThermoScientific, Wilmington, DE). Each concentrated sample was taken out and diluted 1:20 into Dulbecco's phosphate buffered saline (DPBS, without potassium and calcium; Invitrogen, Carlsbad, CA). The samples were monitored for precipitation, and each sample was vortexed for 5 min and centrifuged at 13,000 rpm for 2 min. The OD of each DPBS supernatant was measured to determine peptide concentration at saturation.

Pharmacokinetic evaluation

Primate studies and sample collection

Evaluation of plasma half-life and generation of major metabolites was performed at the Simian Conservation Breeding and Research Center (SICONBREC, Makati City, Philippines) in cynomolgus monkeys (*Macaca fascicularis*). For each analog (Cp20, peptides 3 and 14) two healthy animals were sedated and injected intravenously with 2 mg/kg of the compound (dissolved in saline for injection). Blood samples (1–2 mL) were collected immediately before and at various time points after compound injection (2, 5 and 30 min; 1, 2, 4, 6, and 24 h) in EDTA-coated Vacutainer tubes to prevent coagulation and complement activation, and centrifuged at ~800 × *g* for 10 min to obtain plasma. Plasma samples were immediately frozen and shipped to the University of Pennsylvania for further analysis. All NHP studies were performed in accordance with animal welfare laws and regulations.

Analysis of plasma samples

Compstatin analogs were extracted from plasma samples using solid phase extraction (SPE) and analyzed by reversed phase ultra performance liquid chromatography coupled to high definition mass spectrometry (UPLC-HDMS) as described in Supplementary Methods.

Determination of plasma half-life

Calibration curves were prepared on the day of the analysis by spiking compstatin analogs (Cp20, peptides 3 and 14) into freshly thawed plasma from untreated cynomolgus monkeys at final concentrations of 0.5, 1, 2, 4, and 8 μM. All calibration samples were subjected to SPE and measured using UPLC-HDMS as described above. MS peak areas were determined by integration and plotted against the concentration, resulting in calibration curves that

showed good linearity with regression coefficients (R^2) greater than 0.993. For the pharmacokinetic analysis, the plasma concentration (C_p) at each time point was calculated from the extracted peak area of each peptide using the corresponding standard curve. The elimination constant (k_e) and plasma half-life ($t_{1/2}$) were determined from the slope of the terminal elimination phase (1–24 h) using the following equations:

$$\ln(C_p) = \ln(C_{p0}) - k_e \times t, \text{ and } t_{1/2} = 0.693/k_e$$

Determination of C3 levels

The plasma concentration of C3 in individual cynomolgus monkeys used in this study was determined by ELISA as described in Supplementary Methods.

Results

Solution structure of compstatin Cp10

Our previous studies revealed that backbone N-methylation (Gly8Sar) within the cyclic core region of compstatin favorably influences both the kinetic association rate and binding entropy, thereby contributing to the increased affinity of analogs Cp10 and Cp20 for C3 (Qu et al. 2011). Given the significant differences between the solution and bound conformers of earlier compstatin analogs (Fig. 2) (Janssen et al. 2007), we hypothesized that methylation of Gly8 might stabilize a solution conformation that is structurally reminiscent of the compact, bound conformation. We thus determined the solution conformation of an N-methylated compstatin analog using NMR and also performed molecular dynamics (MD) simulation *in silico*. For the NMR studies, Cp10 was preferred over Cp20 for this purpose due to its better solubility at pH 6, the condition that was previously used to determine the NMR structure of the original compstatin (Morikis et al. 1998). A total of 204 distance restraints derived from observed inter-proton nuclear Overhauser effects (NOEs) were used in a simulated annealing molecular dynamics calculation to determine the structure of Cp10 (Fig. 2). The resulting 20 lowest-energy structures are presented in Fig. 2A and their structural statistics are listed in Supplementary Table 1. No consistent NOE restraint violations were observed in those structures.

The solution structure of Cp10 is compact and dominated by two consecutive β-turns (Fig. 2A and B). The first one involves residues Cys2-Gln5 and the second comprises residues Trp(Me)4-Trp7. Both β-turns were identified by the lack of helicity in these regions combined with the proximity (<7 Å) of the C_α atoms of the respective terminal residues. Residues Trp7-His10 form a relatively linear and extended stretch that is followed by a bend between residues His10 and Arg11. The three-dimensional structure of the peptide is centered upon the first β-turn, which is constrained by multiple NOE contacts between residues Trp(Me)4 and Gln5, and all the residues in the peptide with the exception of Cys2 and His10. The Cys2-Cys12 disulfide bond (supported by NOEs between Cys12 H_N and H_α atoms and Cys2 Hβ atoms) fixes the relative position of the termini (Fig. 2A). The indole rings of Trp(Me)4 and Trp7 are proximal (on average 5.7 ± 0.1 Å apart), as evidenced by the NOE signals detected between Trp(Me)4 $H_{\eta 2}$ and Trp7 $H_{\zeta 3}$, Trp7 H_α and Trp(Me)4 $H\beta_1$, and Trp7 $H_{\varepsilon 3}$ and Trp(Me)4 $H\beta_1$ (Fig. 2A). Additionally the indole ring of Trp7 and the side chain amide nitrogen of Gln5 are close together (on average 3.6 ± 0.1 Å apart), as are the indole ring of Trp(Me)4 and the imidazole ring of His10 (on average 3.8 ± 0.1 Å apart; Fig. 2A). 87.5% of amino acids in the lowest energy set of structures were in the allowed regions of the Ramachandran plot, as established using PROCHECK-NMR software (Laskowski et al. 1993). All residues were determined to be in L conformations, and no mirror images resulted from the structure calculations.

The NOEs detected and assigned for the Cp10 sample were evaluated against the lowest-energy solution structure of the original compstatin (Fig. 2C) ensemble (PDB entry 1A1P; this single structure will be referred to as "free compstatin") (Morikis et al. 1998). They were also evaluated against the crystal structure of compstatin analog 4W9A (Fig. 1C) bound to complement fragment C3c (namely the peptide segment from the PDB entry 2QKI, henceforth referred to as "bound 4W9A") (Janssen et al. 2007). Protons were added to bound 4W9A using Xplor-NIH, and NOEs of Cp10 that are incompatible with the structures of free compstatin and bound 4W9A were identified (Supplementary Fig. 1). Whereas the backbone atoms of conserved residues in Cp10 and bound 4W9A did not superimpose any better than those of free compstatin and bound 4W9A as judged by root mean square deviation (RMSD) measurements (Supplementary Fig. 2A–C), both a visual comparison (Fig. 2C–E) and further quantitative analysis (Supplementary Fig. 2D and E) indicated that the solution structure of Cp10 appears more compact in comparison to the open solution structure of free compstatin, primarily as a result of the peripheral β-turns. Thus, atomic distances between the disulfide bond and the conserved and key C3-binding residue Trp7 were more similar to bound 4W9A than to free compstatin (Supplementary Fig. 2D and E). Moreover the surface-accessible area of Cp10 is roughly 20% smaller than free compstatin (1380 $Å^2$ *vs.* 1740 $Å^2$). In summary Cp10 in solution adopts a less elongated structure than free compstatin consistent with a lower entropic cost of adopting the compact conformation of bound compstatin observed in bound 4W9A.

These findings were further supported and extended by computational studies, in which we compared the MD trajectories of analog Cp20 (also containing Sar8) with that of non-backbone-methylated analog 4W9A in relation to the C3c-bound conformer (Supplementary Fig. 3). Whereas both analogs switched between distinct conformers during the MD simulation period of 100 ns, the deviation from the bound forms (measured as the RMSD of the side chain of Trp7) was generally higher for 4W9A when compared to Cp20 (~6 Å *vs.* 4 Å). In addition, Cp20 reached conformational states with a RMSD < 2 Å for a longer time and with higher frequency (Supplementary Fig. 2), thereby indicating an increased preference of Cp20 for bound-like states, similar to what was observed for Cp10 in the NMR study. In summary, both the NMR and MD analyses largely support the stabilization of more bound-like conformers in analogs with backbone N-methylation at position 8 and validated the use of such a scaffold for subsequent optimization steps.

Structure/activity of N-terminal extensions

Although the bound structure of Cp20 has not yet been resolved, the overall similarity of the peptide core between Cp20 and the earlier analog 4W9A that was used in the available co-crystal structure strongly indicates a homologous binding mode. We therefore used molecular modeling and docking approaches (see also next section) to prepare a model of Cp20 bound to its target protein fragment C3c. Computational analysis of this complex confirmed that the methyl group of Sar8 forms a contact with the oxygen atom of G489 in C3c (distance ~4.0 Å). Yet analysis of the binding site also revealed the existence of a hydrophobic area on C3c that may be exploited *via* N-terminal extension of the peptide ligand. While not buried in the binding pocket of C3c, the N-terminus of compstatin has previously been protected by an acetyl moiety primarily to improve peptide stability; however, such capping also had a beneficial effect on the inhibitory potency. Based on the current lead compound Cp20, we therefore evaluated the effect of replacing the N-terminal acetyl moiety on target binding (Table 1). For this purpose, analogs were subjected to quantitative kinetic profiling for their binding

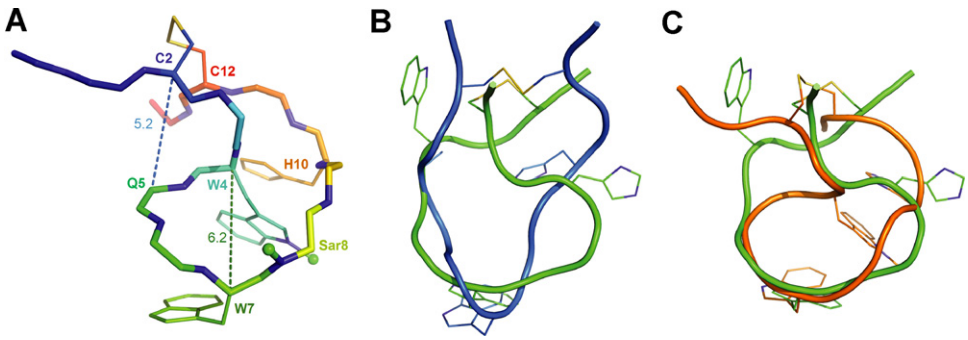

Fig. 2. Structural comparison of free and C3c-bound compstatin analogs. (A) Lowest energy NMR structure of Cp10. The two β-turns between residues Cys2-Gln5 and Trp(Me)4-Trp7 are indicated as dotted lines with the labels depicting the atomic distances between the C_α atoms. The methyl groups of Trp(Me)4 and Sar8 are indicated by green spheres. (B) Superimposed structures of compstatin (PDB 1A1P, blue) in solution and analog 4W9A when bound to C3c (PDB 2QKI, green). (C) Superimposed solution structure of Cp10 (orange) and C3c-bound 4W9A (2QKI; green). Side chains of residues Cys2, Val/Trp(Me)4, Trp7, His10 and Cys12 are shown as sticks. All structure visualizations were prepared in PyMOL (www.pymol.org). (For interpretation of the references to colour in this figure legend, the reader is referred to the web version of the article.)

to C3b and compared to the clinically used analog 4(1MeW) and to Cp20 (Table 1, Fig. 3, Supplementary Fig. 4). Indeed, substitution of the terminal acetyl with a shorter methyl group (peptide 1) led to a drop in affinity by almost an order of magnitude, below that of 4(1MeW), thereby confirming the importance of N-terminal capping. In contrast, capping with a glycine residue (peptide 2) improved the dissociation rate (k_d) yet slightly lowered the association rate (k_a), leading to only a very small net change in affinity (compared to Cp20). Importantly, though, N-methylation of Gly to Sar (peptide 3) restored the association properties while retaining the beneficial dissociation value, which produced a lead compound with significantly improved affinity (K_D = 1.6 nM; Table 1).

Encouraged by the potential benefit of N-terminal optimization, we screened additional Cp20-based analogs with natural (peptides 4–8), methylated (peptides 9–13) and D-amino acids (peptides

Table 1
Evaluation of C3b interaction profiles for a series of compstatin analogs with N-terminal modifications (Xaa0-Xaa1-[Cys-Val-Trp(Me)-Gln-Asp-Trp-Sar-Ala-His-Arg-Cys]-mIle-NH_2).

Peptide[a]	Xaa0	Xaa1	k_a (10^6/Ms)	k_d (10^{-3}/s)	K_D (nM)
4(1MeW)[b]	–	–	1.1 ± 0.1	11.3 ± 0.9	10.3 ± 1.5
Cp20[c]	Ac	Ile	1.9	4.0	2.4
1	Me	Ile	1.3 ± 0.3	24.8 ± 7.3	18.6 ± 3.5
2	Gly	Ile	1.2 ± 0.3	2.9 ± 0.2	2.5 ± 0.5
3	Sar	Ile	1.9 ± 0.5	2.9 ± 0.3	1.6 ± 0.3
4	Tyr	Ile	2.1 ± 0.3	2.5 ± 0.1	1.2 ± 0.1
5	Phe	Ile	2.1 ± 0.4	3.3 ± 0.3	1.6 ± 0.2
6	Arg	Ile	1.7 ± 0.2	2.9 ± 0.2	1.7 ± 0.2
7	Trp	Ile	1.6 ± 0.1	3.6 ± 0.2	2.2 ± 0.2
8	Thr	Ile	1.2 ± 0.1	3.1 ± 0.2	2.6 ± 0.3
9	Tyr(Me)	Ile	2.3 ± 0.4	2.6 ± 0.1	1.2 ± 0.2
10	mPhe	Ile	1.6 ± 0.2	2.9 ± 0.3	1.8 ± 0.3
11	mVal	Ile	1.8 ± 0.3	3.5 ± 0.6	1.9 ± 0.1
12	mIle	Ile	1.6 ± 0.2	3.7 ± 0.3	2.4 ± 0.5
13	mAla	Ile	1.4 ± 0.2	3.4 ± 0.3	2.5 ± 0.6
14	DTyr	Ile	2.8 ± 0.5	1.4 ± 0.1	0.5 ± 0.1
15	DPhe	Ile	2.3 ± 0.3	2.6 ± 0.0	1.1 ± 0.1
16	DTrp	Ile	2.0 ± 0.2	2.4 ± 0.1	1.2 ± 0.1
17	DCha	Ile	1.8 ± 0.5	2.7 ± 0.4	1.5 ± 0.2
18	DAla	Ile	1.4 ± 0.3	3.4 ± 0.4	2.5 ± 0.4
19	Ac	Trp	3.8 ± 0.3	1.7 ± 0.3	0.5 ± 0.1
20	Tyr	Gly	2.1 ± 0.3	7.3 ± 1.4	3.5 ± 0.3

[a] The following analogs were selected as potential lead compounds: peptide 3 = Cp30, peptide 14 = Cp40.
[b] Analog 4(1MeW) was included as a standard in all analyses; it does not follow the Cp20 template (Fig. 1C).
[c] Base compound for N-terminal modifications; binding/potency values from previous publication (Knerr et al. 2011).

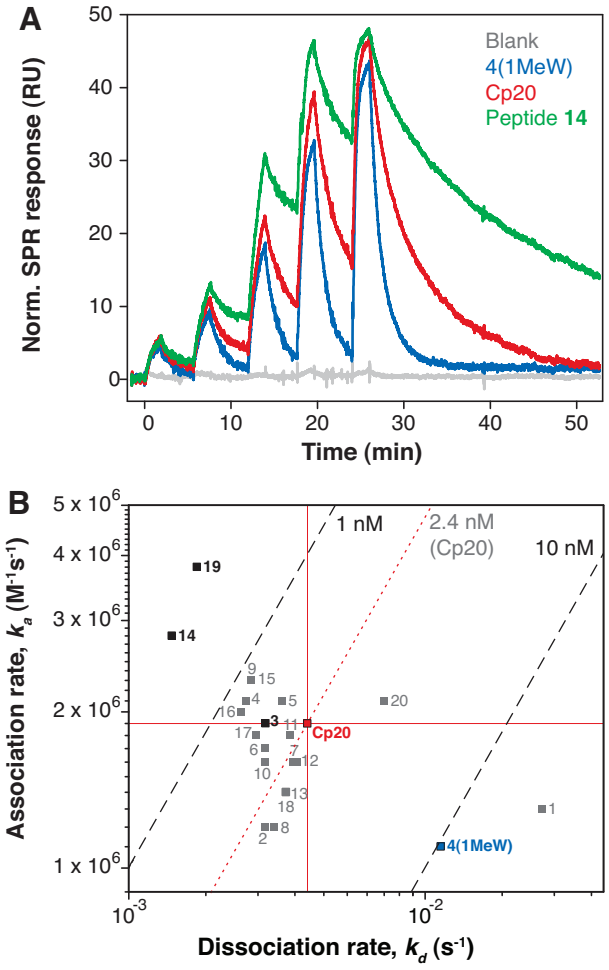

Fig. 3. Interaction of compstatin analogs with C3b. (A) Kinetic profiles of compstatin lead compounds 4(1MeW), Cp20, and peptide 14 (Cp40) as determined by single cycle kinetic analysis using surface plasmon resonance. Binding data and kinetic fits to a 1:1 model for all tested analogs can be found in Supplementary Fig. 4. (B) Rate plot of peptides 1-20 as well as reference compounds 4(1MeW) and Cp20 with isoaffinity lines shown as dashed lines. Benchmark lines for the rate constant and affinity of Cp20 are highlighted in red. Compounds selected for subsequent studies are marked as black squares. (For interpretation of the references to colour in this figure legend, the reader is referred to the web version of the article.)

Table 2
Complement inhibition potency of selected compstatin analogs.

Peptide[a]	Xaa0	Xaa1	IC_{50} (nM)
4(1MeW)	–	–	132 ± 7
1	Me	Ile	180 ± 17
2	Gly	Ile	113 ± 16
3	Sar	Ile	82 ± 14
4	Tyr	Ile	72 ± 10
14	DTyr	Ile	66 ± 8
19	Ac	Trp	N/D[b]

[a] 4(1MeW) was included as a standard in all analyses.
[b] Peptide 19 could not be sufficiently solubilized.

14–18) at position Xaa0 (Fig. 1B; Table 1). The set included representative hydrophobic, hydrophilic, and charged side chains. All tested compounds showed strong binding (K_D < 20 nM), with the k_a values ((1–4) × 10^6 M^{-1} s^{-1}) showing less variability than k_d values ((1–25) × 10^{-3} s^{-1}) across the entire panel (Table 1, Fig. 3B). Notably, all analogs followed a 1:1 Langmuir kinetic model when screened for binding to C3b, thereby strongly supporting the presence of a single high-affinity binding site. In general, D-amino acids with hydrophobic side chains appeared to be favored over the acetyl (Ac) moiety of Cp20. Among those, peptide 14 with a DTyr at that position was the most potent, with a subnanomolar affinity (K_D = 0.5 nM; Table 1) and the slowest dissociation rate of the panel. The affinity of peptides in which Ac was replaced by other amino acids fell between that of peptides 1 and 14, with most analogs clustering around the profile of Cp20 (Fig. 3B). Tyrosine appears generally preferred since all peptides with N-terminal Tyr, its O-methyl analog and its D-isoform ranked among the best binders with affinities around or below 1 nM. In contrast, residues with shorter side chains like Gly, Thr, or Ala derivatives seem less favorable and do not improve the affinity compared to Cp20. Although extended studies would be needed to confirm individual trends, replacement of the capping Xaa0 residue appears to be well-tolerated for a wide range of amino acid residues with properties ranging from hydrophobic to charged, and may be used for further optimization or labeling of compstatin.

Selected analogs were further subjected to an established complement inhibition ELISA to further test and validate their potency; while the dynamic range of this assay did not allow for the same resolution, the ranking was highly comparable to the SPR results with peptide 14 being the most potent and peptide 1 being the weakest inhibitor. Again, in the series of peptides 1–3, Sar was preferred over Gly as an N-terminal capping moiety, whereas methylation led to a profound drop in potency (Table 2).

Computational analysis

In order to provide structural evidence for the observed effects on binding affinity and generate a computational model for predicting novel analogs, we performed extended docking analyses. Initially, the docking strategy was validated using the data set from the screening of N-terminally modified analogs of Cp20 (peptides 1–18; Table 1). For this purpose, the compounds were prepared *in silico*, docked into the compstatin binding pocket of human C3c (Janssen et al. 2007), and the binding free energy (ΔG) was calculated and compared to the SPR affinity-derived values by determining the Pearson's correlation coefficient (R; Supplementary Fig. 5). The overall correlation between experimental and calculated ΔG values was 0.46 based on five independent docking studies over the entire data set (Supplementary Fig. 5). Out of the 19 analogs in the data sets, three peptides bearing either a very short moiety (methyl; peptide 1) or aromatic natural amino acid (peptides 5 and 7) showed a significantly higher deviation; when these analogs were excluded, the correlation increased to 0.69 (Supplementary Fig. 5). These results indicate that this docking approach may be developed into a valuable tool for guiding and validating structural optimization of compstatin.

Table 3
Solubility of selected analogs in clinically relevant solvents, and apparent hydrophobicity.

Peptide	Solubility[a]		Hydrophobicity[b]
	WFI (mg/mL)	DPBS (mg/mL)	Retention (min)
4(1MeW)	>50	3.5	5.09
Cp20	13	2.7	5.33
3	>50	6.9	4.60
14	>50	0.8	4.73
19	N/D[c]	(<0.2)[c]	N/D[c]

[a] Measured as OD (280 nm) at saturation; WFI: water for injection; DPBS: Dulbecco's phosphate buffered saline.
[b] Measured as retention time during UPLC analysis on a C18 column.
[c] Peptide 19 could not be solubilized at 100 μM or above in PBS during ELISA studies and was therefore not further evaluated.

A more detailed analysis of the docked peptides indicated that most of the N-terminally modified compstatin analogs formed additional contacts with a polar area and a shallow pocket on C3c. For example, the polar area involving Asp349, Ser388 and Ser437 of C3c interacts with the N-terminal amino group of DTyr in peptide 14 (Fig. 4A). In contrast, such a polar interaction is not favored for peptides carrying natural amino acid residues at this position, as exemplified for peptide 4, due to a different orientation of the amino group (Fig. 4A). Furthermore, the side chain of the elongated amino acid (DTyr) in peptide 14 forms additional hydrophobic contacts with Leu454 and Leu492 in the shallow extended pocket on C3c. Finally, the hydroxyl group of DTyr formed a weak hydrogen bond with Asn452 of C3c. A combination of those effects is likely to contribute to the observed subnanomolar binding affinity of peptide 14.

To further explore distinct strategies of addressing the N-terminal pocket, we designed two analogs where an aromatic residue is either located at position Xaa0 or Xaa1 (peptides 19 and 20; Table 1). Based on the computational model developed above, the side chain of the new Trp in peptide 19 was predicted to fit nicely into the hydrophobic binding pocket (Fig. 4B), whereas a short flexible Gly linker was chosen in peptide 20 to allow a better orientation of the Tyr side chain when compared to the homolog peptide 4. While peptide 20 showed a threefold weaker binding affinity than peptide 4, peptide 19 reached sub-nanomolar binding affinities (K_D = 0.5 nM; Table 1), making it as potent as peptide 14. Together, these studies strongly imply the importance of a properly oriented hydrophobic residue adjacent to Cys at position 2.

Solubility

While the presence of three acidic or basic residues (Asp6, His10, Arg11) in most compstatin analogs contributes to a generally favorable solubility in aqueous solutions, their zwitterionic nature may negatively affect solubility in buffered solutions. We therefore evaluated and compared the solubility of selected compounds in two clinically relevant solvents, *i.e.*, water for injection (WFI) and Dulbecco's PBS (DPBS; Table 2). In addition, the ultra performance liquid chromatography (UPLC) retention time of these peptides on a C18 column was measured to reflect their apparent relative hydrophobicity (Table 3, Supplementary Fig. 6). As expected, the solubility in WFI was excellent, with values exceeding 50 mg/mL for all compounds with the exception of Cp20. In general, the solubility in DPBS was significantly lower for all analogs. The decreased solubility of Cp20 in both solvents, as compared to 4(1MeW), is considered a consequence of its hydrophobicity arising from two N-methylations (positions 8 and 13) and the C-terminal

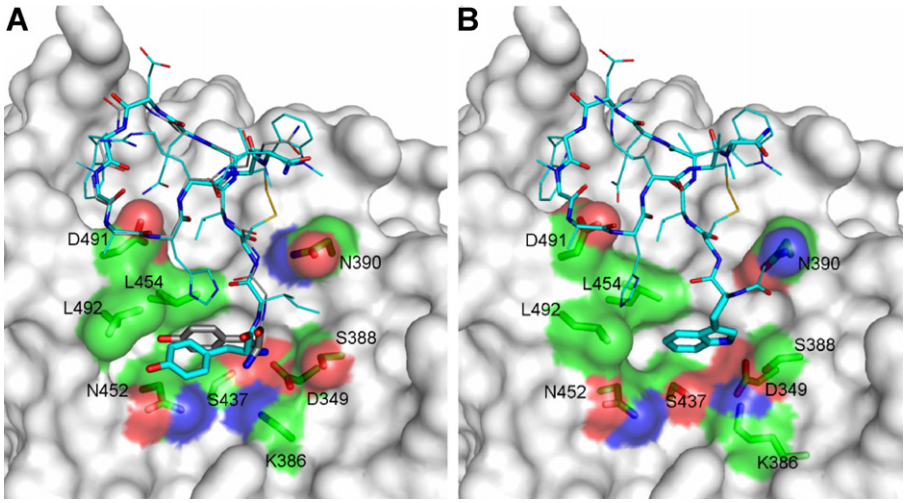

Fig. 4. Docking of compstatin analogs into the binding site of C3c. (A) Docked conformation of peptide 14 (cyan) and peptide 4 (gray). Other D-amino acid residues at the C-terminus have a similar conformation as peptide 14 in the docked models. Side chains of other residues in peptide 4 were omitted for clarity. (B) Docking conformation of peptide 19. (For interpretation of the references to colour in this figure legend, the reader is referred to the web version of the article.)

Thr-to-Ile substitution. The replacement of the N-terminal acetyl moiety in 4(1MeW) and Cp20 by uncapped amino acid residues induced a significant gain in hydrophilicity for peptides 3 and 14 and restored their high solubility in WFI (>50 mg/mL). However, the incorporation of a hydrophobic DTyr at its N-terminus negatively impacted the solubility of peptide 14 (0.8 mg/mL) in DPBS. In contrast, the presence of a small N-terminal Sar in peptide 3 largely improved its solubility in DPBS (6.9 mg/mL), rendering this peptide almost twice as soluble as the clinically-used 4(1MeW) analog.

Plasma half-life

Peptidic drugs are often hampered by comparatively fast elimination from plasma, which may be highly restrictive in clinical applications that rely on constant systemic drug levels (*e.g.*, PNH in the case of complement inhibitors). We therefore performed a comparative study including Cp20 and the newly developed peptides 3 and 14, in which cynomolgus monkeys were intravenously injected with 2 mg/kg of each analog and the plasma levels were assessed by LC–MS over a period of 24 h. Interestingly, all tested analogs followed a similar biphasic elimination profile, in which the plasma levels dropped more rapidly within the first hour after injection and then followed a much slower decrease throughout the later time points (Fig. 5A). Intriguingly, the peptide concentrations at which the kinetic change occurred were highly similar to that of the expected physiological plasma levels of the target protein C3. Indeed, measurement of the C3 levels in the involved monkeys by ELISA (4.9–12.8 μM) confirmed that the initial drop in compstatin levels slowed down within the determined range of C3 (Fig. 5A; Supplementary Table 2). These observations suggest a target-driven elimination model, where tight binding to the abundant target C3 largely influences peptide excretion. Indeed, when the plasma half-life was calculated based on the terminal log-linear portion (1–24 h), a direct correlation to the binding affinity for C3 could be observed with half-life values of 9.3, 10.1 and 11.8 h for Cp20, peptide 3 and peptide 14, respectively (Fig. 5B).

Given the strong apparent dependence of the major elimination phase with the binding affinity, the translation of these NHP-based studies to the human system may be critically influenced by the differential affinity of these compstatin analogs for human and NHP C3. We therefore measured the binding profiles of Cp20 and peptides 3 and 14 for C3 from humans and three relevant NHPs (cynomolgus monkey, rhesus monkey, baboon) using SPR. Both the affinity and kinetic profiles for all analogs were highly comparable between human and NHP C3 (Fig. 5C; Supplementary Fig. 7). In summary, these studies suggest comparatively slow and target-driven elimination kinetics that may be further improved by optimizing the binding affinity to C3, and indicate a strong potential for extrapolation of the NHP model to the human system.

Discussion

In this study, we describe novel analogs of the clinical complement inhibitor compstatin with sub-nanomolar affinity, favorable solubility profiles and improved pharmacokinetic properties. In addition, we shed light on important structure–activity relationships that may well guide the future development of this drug candidate. During the past two decades, compstatin and its analogs have proven to be highly valuable inhibitors for testing and dissecting the influence of complement activation pathways in disease models and in biomaterial-related studies. Their high potency and comparatively small size in a field that is dominated by antibodies and recombinant proteins also render them attractive compounds for clinical development. Besides local applications, *e.g.*, intravitreal injection in the case of ongoing clinical trials for AMD (Alcon Research; Potentia Pharmaceuticals), the promising outcomes of compstatin-mediated complement inhibition in an NHP model of sepsis and in an *ex vivo* model of hemodialysis suggest a high clinical value for systemic administration of the peptidic drug (Kourtzelis et al. 2010; Silasi-Mansat et al. 2010). However, localized and systemic applications impose distinct demands on physicochemical and pharmacokinetic properties of a compound, and the improvements described here are therefore likely to extend the use of compstatin analogs in clinical applications.

Previous studies described critical aspects of the structure–activity relationship of compstatin, including the importance of the cyclic structure, overall hydrophobicity, N-terminal capping, or indole groups at positions 4 and 7 (Katragadda et al. 2006; Magotti et al. 2009; Ricklin and Lambris 2008). They also revealed significant conformational differences between compstatin in solution and bound to its target (Janssen et al. 2007), thereby indicating the necessity of an induced fit for building the inhibitory complex. In our previous work on effects of backbone N-methylation, we showed a measurable improvement in complex formation (*i.e.*, association rate constant) for methylation at position 8 (Gly-to-Sar) (Qu et al. 2011). Thermodynamic and kinetic assessment led

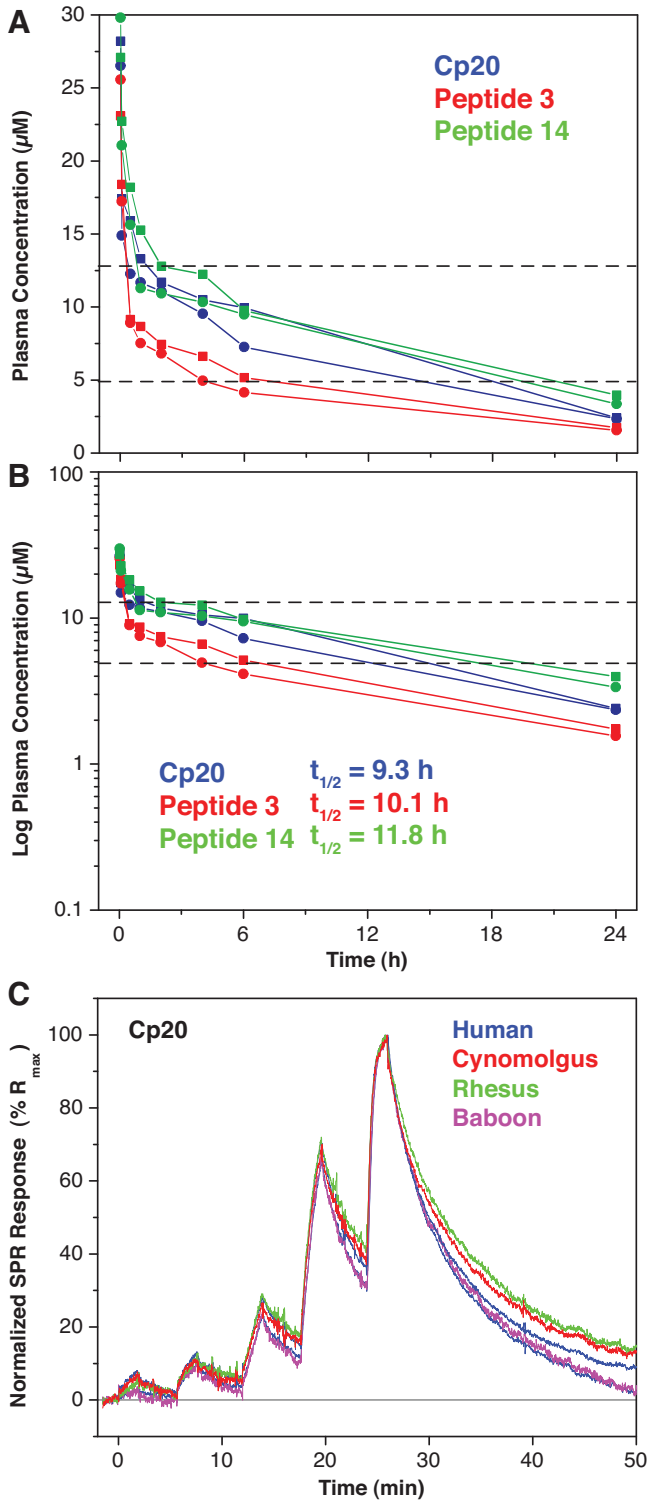

Fig. 5. Pharmacokinetic assessment of compstatin analogs in non-human primates. (A) Linear plot of peptide level over time after *i.v.* bolus injection of 2 mg/kg in cynomolgus monkeys, showing a biphasic model with a rapid initial elimination phase followed by a slow log-linear terminal phase. (B) Calculation of the plasma elimination half-life ($t_{1/2}$) from the terminal phase (1–24 h). Dashed lines mark the range of measured plasma levels of the target protein C3 in both panels A and B. (C) Superimposition of kinetic binding profiles of analog Cp20 to immobilized C3 from humans, baboons, cynomolgus monkeys and rhesus monkeys as assessed by SPR.

us to hypothesize that the introduction of a methyl group to the backbone would change the overall solution conformation of compstatin to one resembling the compact bound structure (Janssen et al. 2007; Qu et al. 2011). Indeed, the NMR studies performed here supported this hypothesis since an analog containing N-methyl group at position 8 (*i.e.*, Cp10) adopted a preferred conformation in solution that is distinct from the one published previously for an analog without the modification. Specifically, the early analog was characterized by a β-turn in the center of the ring structure (positions 5–8), giving it an elongated and open U-shaped appearance (Morikis et al. 1998). In contrast, the bound form is more compact, appearing twisted and O-shaped as a result of a shift of the turns to peripheral areas close to the disulfide (*e.g.*, positions 8–11) (Janssen et al. 2007). Importantly, the methyl group at position 8 in Cp10 seems to disfavor a central turn but favors alternative peripheral turn formation, in particular in the area between residues 2–5 and 4–7. While not entirely recapitulating the bound conformation, the resulting structure is indeed more twisted and 'closed'; it thereby likely reduces the extent of the conformational rearrangement and loss of entropy required for an induced fit and improves the association rate. Other studies have shown that N-methylation induces or shifts conformational preferences (Chatterjee et al. 2008). It is important to note that the enhanced association rate was preserved (or even further enhanced) in the vast majority of Cp20 derivatives tested in this study, which strongly supports the importance of N-methylation at position 8 for the potency of compstatin analogs and hence suggests maintenance of this scaffold for future optimization steps.

Given the high importance of the cyclic ring core, the majority of earlier optimization efforts were focused on modifying the core residues between cysteines 2 and 12 (Magotti et al. 2009; Ricklin and Lambris 2008). The co-crystal structure further supported this strategy as it revealed that the N- and C-terminal residues of analog 4W9A formed few contacts with C3c and mainly pointed out into the solvent (Janssen et al. 2007). Yet in the case of the C-terminus, our recent analyses demonstrated that modification of position 13, especially the introduction of N-methylated amino acids, can improve the target binding affinity (Qu et al. 2011). Similarly, capping of the N-terminal Ile with an acetyl moiety not only improved the stability towards peptidases but also led to a threefold increase in activity (Sahu et al. 2000). Computational simulation studies have also identified the N-terminus as a potential site of optimization, but have not yet resulted in analogs with improved activity (Bellows et al. 2010; Lopez de Victoria et al. 2011). The binding site analysis performed in this study revealed additional potential binding areas on C3c near the N-terminus of bound analog 4W9A and suggested extension rather than replacement of Ile1 as a novel strategy for improving the binding affinity. Indeed, replacing the acetyl capping moiety (termed position 0 to maintain the traditional compstatin numbering scheme) significantly influenced the binding affinity to C3b and produced the most active compstatin analogs to date. In fact, peptide 14 features a binding affinity that is 5600-fold stronger than the one described for the original compstatin (Sahu et al. 2000); compared to more recent analogs, the improvement is still 20-fold over the clinically used analog 4(1MeW) and almost fivefold over the previous lead Cp20 (Table 1). Whereas the inhibitory potency towards the classical pathway of complement was also greatly improved (from 12 μM reported for the original compstatin to 66 nM; Table 2), the comparison between studies is more difficult as the assay is directly dependent on the plasma level of C3 and the serum dilution. Since full inhibition requires saturation of the abundant target C3 (~6 μM in plasma; ~75 nM in the assay), the dynamic range and potential for improving the IC_{50} is much lower when compared to the gains in K_D. Importantly, though, an improvement of the binding affinity

not only affects the inhibitory potency but also appears to influence the pharmacokinetic properties (see below).

When comparing the effect of various hydrophobic, hydrophilic, N-methylated and D-amino acids for replacing the Ac group in Cp20, our data indicate that D-amino acids with aromatic side chains are preferred. The docking studies showed that N-terminal extension generally improved the affinity through additional polar and non-polar interactions involving both the peptide's free amino group and the side chain of the Xaa0 residue. In the case of aromatic D-amino acids, the terminal amino groups were more favorably oriented and the side chains were involved in additional hydrophobic interactions. As a consequence, the large affinity gain of peptide 14 can be attributed to polar contacts of the free amino group of DTyr, interactions of the aromatic ring with the hydrophobic pocket on C3c and hydrogen bonding of the Tyr hydroxyl group. Overall, the docking study showed a good correlation between the calculated and experimentally determined free energy values and may be utilized to screen for and predict beneficial modifications of the Cp20 scaffold.

Selecting non-proteinogenic amino acids at position Xaa0, such as Sar in peptide 3 or DTyr in peptide 14, is expected to afford the additional benefit of maintaining protection against exopeptidases. Whereas the cyclic structure of compstatin renders the peptide core comparatively stable against proteolysis, an unprotected L-amino acid residue at the N-terminus was shown to be susceptible to cleavage (Sahu et al. 2000). While acetylation was able to prevent degradation in subsequent analogs (Sahu et al. 2000), both N-methylation and the use of D-amino acids are known to provide equal stability against degradation in physiological environments (Chatterjee et al. 2012; Hlavacek et al. 2011; Linde et al. 2008; Nestor 2009; Tugyi et al. 2005).

Alongside metabolic stability, the solubility of peptidic drugs also defines their use in clinical applications (Nestor 2009). Previous optimization steps tended to increase the hydrophobicity of compstatin analogs, which had beneficial effects on the binding affinity and inhibitory potency but negatively influenced solubility (Katragadda et al. 2006; Magotti et al. 2009; Qu et al. 2011). Although the presence of basic amino acids (His10, Arg11) generally provides high solubility in slightly acidic solvents like WFI, pH adjustment to physiological levels (as in DPBS) leads to a sharp drop in solubility. Indeed, both the clinically used analog 4(1MeW) and the previous lead compound Cp20 showed such pH-dependent solubility profiles, with Cp20 featuring high hydrophobicity and comparatively low solubility in WFI and DPBS. The introduction of DTyr in peptide 14 did not prove beneficial for solubility in DPBS, yet largely improved the WFI solubility when compared to Cp20; these changes in the solubility profile can likely be attributed to the replacement of the N-terminal acetyl moiety with an uncapped amino acid, in which the new analog reacts more sensitively to pH changes. Interestingly, the introduction of Sar at the same position in peptide 3 led to a highly beneficial improvement of solubility in both solvents, even though the overall peptide hydrophobicity was similar to peptide 14. Whereas N-methylation by itself may influence aqueous solubility *via* reduction of intermolecular hydrogen bonds and electron-inducing effects (Bose et al. 2010), the side chain hydrophobicity appears to largely contribute to the observed changes in the tested panel. This high solubility of peptide 3 in physiologically adjusted solvents may prove beneficial for systemic administration (*e.g.*, bolus injection) since the necessary peptide concentrations to block the abundant plasma protein C3 may be reached with a much smaller injection volume. On the other hand, the solubility of peptide 14 in buffered solutions is still considered sufficiently high for many systemic applications. In the case of local administration, lower solubility may even prove advantageous, since it might allow for slow-release applications; indeed, such sustained-release kinetics from pH-dependent microprecipitates have been indicated for intravitreal injection of compstatin analogs in AMD (Chi et al. 2010; Yehoshua et al. 2011) and have also been used for subcutaneous depositing of insulin (Ashwell and Home 2001).

Irrespective of the solubility and the administration method, however, disfavored pharmacokinetic profiles due to rapid elimination from plasma still impose a major limitation for the clinical use of peptidic drugs. Previous preliminary studies with compstatin analogs, including 4(1MeW), indicated fast elimination profiles with plasma half-life values of less than 2 h (unpublished observations). Strikingly, though, our pharmacokinetic analysis of the advanced compstatin analogs used in this study revealed surprisingly low elimination profiles in NHPs with highly beneficial plasma half-life values of up to almost 12 h. Although the biphasic plasma profile after *i.v.* bolus injection resembles a two compartment model with compound distribution, there are strong indications that these compstatin analogs actually follow a target-driven model due to the fact that C3 is a highly abundant plasma protein. Most tellingly, the high initial plasma concentrations rapidly drop until they reach the determined plasma levels for C3 (within 1 h), which is followed by a much slower terminal elimination phase. In addition, this second phase is clearly dependent on the binding affinity for C3, with peptide 14 showing both the strongest K_D and slowest half-life values (Table 1, Fig. 5B). Finally, a comparable pharmacokinetic analysis of Cp20 in rodents resulted in very rapid plasma elimination (data not shown); since compstatin only binds to human and NHP C3 but not rodent C3 (Sahu et al. 2003), this observation further supports the hypothesis that binding to plasma C3 rather than distribution between compartments is responsible for the biphasic profile and slow terminal elimination phase. In this context, we also re-investigated the relative binding affinities of the new compstatin analogs to C3 from humans and three NHPs that are often used in preclinical studies. Similarly to previous studies with original compstatin (Sahu et al. 2003), we found highly comparable activities for the binding of all three tested analogs (Cp20, Peptides 3 and 14) to C3 from humans, baboons, cynomolgus monkeys and rhesus monkeys. While this is consistent with the high sequence similarity of the compstatin-binding site between human and various NHP species (Supp. Fig. 8), it also indicates that our pharmacokinetic assessment in NHPs likely translates into the human situation. Additional studies may need to be performed to confirm the pharmacokinetic hypothesis of a target-driven model, as well as to investigate the major routes of excretion and the potential generation of metabolites. Nonetheless, the current data clearly indicate that Cp20 and the newly disclosed peptides 3 and 14 all feature beneficial pharmacokinetic profiles suitable for systemic applications and strongly indicate that further optimization of the binding affinity may improve both the efficacy and pharmacokinetics of future compstatin analogs.

Acknowledgments

This work was supported by National Institutes of Health grants GM62134, AI30040, AI068730, GM097747, and EY020633.

Appendix A. Supplementary data

Supplementary data associated with this article can be found, in the online version, at http://dx.doi.org/10.1016/j.imbio.2012.06.003.

References

Alcon Research, 2011. Evaluation of AL-78898A in Exudative Age-Related Macular Degeneration (AMD). In: ClinicalTrials.gov [Internet]. Bethesda (MD):

National Library of Medicine (US). 2000- [cited 2012 June 1]. Available from: http://clinicaltrials.gov/show/NCT01157065 NLM Identifier: NCT01157065.
Ashwell, S.G., Home, P.D., 2001. Insulin glargine: the first clinically useful extended-action insulin analogue. Expert Opin. Pharmacother. 2, 1891–1902.
Bellows, M.L., Fung, H.K., Taylor, M.S., Floudas, C.A., Lopez de Victoria, A., Morikis, D., 2010. New compstatin variants through two de novo protein design frameworks. Biophys. J. 98, 2337–2346.
Bose, P.P., Chatterjee, U., Hubatsch, I., Artursson, P., Govender, T., Kruger, H.G., Bergh, M., Johansson, J., Arvidsson, P.I., 2010. In vitro ADMET and physicochemical investigations of poly-N-methylated peptides designed to inhibit Abeta aggregation. Bioorg. Med. Chem. 18, 5896–5902.
Chatterjee, J., Gilon, C., Hoffman, A., Kessler, H., 2008. N-methylation of peptides: a new perspective in medicinal chemistry. Acc. Chem. Res. 41, 1331–1342.
Chatterjee, J., Laufer, B., Kessler, H., 2012. Synthesis of N-methylated cyclic peptides. Nat. Protoc. 7, 432–444.
Chi, Z.L., Yoshida, T., Lambris, J.D., Iwata, T., 2010. Suppression of drusen formation by compstatin, a peptide inhibitor of complement C3 activation, on cynomolgus monkey with early-onset macular degeneration. Adv. Exp. Med. Biol. 703, 127–135.
Deal Watch, 2009. Deal watch: Alcon licenses complement pathway inhibitor for macular degeneration. Nat. Rev. Drug Discov. 8, 922.
Emlen, W., Li, W., Kirschfink, M., 2010. Therapeutic complement inhibition: new developments. Semin. Thromb. Hemost. 36, 660–668.
Hlavacek, J., Tykva, R., Holik, J., Bennettova, B., Budesinsky, M., Vlasakova, V., Cerny, B., Slaninova, J., 2011. Oostatic peptides containing D: -amino acids: synthesis, oostatic activity, degradation, accumulation in ovaries and NMR study. Amino Acids.
Janssen, B.J., Halff, E.F., Lambris, J.D., Gros, P., 2007. Structure of compstatin in complex with complement component C3c reveals a new mechanism of complement inhibition. J. Biol. Chem. 282, 29241–29247.
Katragadda, M., Magotti, P., Sfyroera, G., Lambris, J.D., 2006. Hydrophobic effect and hydrogen bonds account for the improved activity of a complement inhibitor, compstatin. J. Med. Chem. 49, 4616–4622.
Knerr, P.J., Tzekou, A., Ricklin, D., Qu, H., Chen, H., van der Donk, W.A., Lambris, J.D., 2011. Synthesis and activity of thioether-containing analogues of the complement inhibitor compstatin. ACS Chem. Biol. 6, 753–760.
Kourtzelis, I., Markiewski, M.M., Doumas, M., Rafail, S., Kambas, K., Mitroulis, I., Panagoutsos, S., Passadakis, P., Vargemezis, V., Magotti, P., Qu, H., Mollnes, T.E., Ritis, K., Lambris, J.D., 2010. Complement anaphylatoxin C5a contributes to hemodialysis-associated thrombosis. Blood 116, 631–639.
Lachmann, P.J., Smith, R.A., 2009. Taking complement to the clinic—has the time finally come? Scand. J. Immunol. 69, 471–478.
Laskowski, R.A., MacArthur, M.W., Moss, D.S., Thornton, J.M., 1993. A program to check the stereochemical quality of protein structures. J. Appl. Crystallogr. 26, 283–291.
Linde, Y., Ovadia, O., Safrai, E., Xiang, Z., Portillo, F.P., Shalev, D.E., Haskell-Luevano, C., Hoffman, A., Gilon, C., 2008. Structure–activity relationship and metabolic stability studies of backbone cyclization and N-methylation of melanocortin peptides. Biopolymers 90, 671–682.
Lopez de Victoria, A., Gorham Jr., R.D., Bellows-Peterson, M.L., Ling, J., Lo, D.D., Floudas, C.A., Morikis, D., 2011. A new generation of potent complement inhibitors of the Compstatin family. Chem. Biol. Drug Des. 77, 431–440.
Magotti, P., Ricklin, D., Qu, H., Wu, Y.Q., Kaznessis, Y.N., Lambris, J.D., 2009. Structure–kinetic relationship analysis of the therapeutic complement inhibitor compstatin. J. Mol. Recognit. 22, 495–505.
Mallik, B., Katragadda, M., Spruce, L.A., Carafides, C., Tsokos, C.G., Morikis, D., Lambris, J.D., 2005. Design and NMR characterization of active analogues of compstatin containing non-natural amino acids. J. Med. Chem. 48, 274–286.
Markiewski, M.M., Lambris, J.D., 2007. The role of complement in inflammatory diseases from behind the scenes into the spotlight. Am. J. Pathol. 171, 715–727.
Morikis, D., Assa-Munt, N., Sahu, A., Lambris, J.D., 1998. Solution structure of Compstatin, a potent complement inhibitor. Protein Sci. 7, 619–627.
Nestor Jr., J.J., 2009. The medicinal chemistry of peptides. Curr. Med. Chem. 16, 4399–4418.
Potentia Pharmaceuticals, 2010. Safety of intravitreal POT-4 therapy for patients with neovascular age-related macular degeneration (AMD) (ASaP). In: ClinicalTrials.gov [Internet]. Bethesda (MD): National Library of Medicine (US). 2000- [cited 2012 June 1]. Available from: http://clinicaltrials.gov/show/NCT00473928 NLM Identifier: NCT00473928.
Qu, H., Magotti, P., Ricklin, D., Lambris, J., 2009a. Development of compstatin-albumin binding peptide conjugates for prolonged peptide half-life. Biopolymers 92, 323.
Qu, H., Magotti, P., Ricklin, D., Lambris, J.D., 2009b. Development of compstatin derivative-albumin binding peptide chimeras for prolonged plasma half-life, Bloomington, IN, U.S.A, pp. 219–220.
Qu, H., Magotti, P., Ricklin, D., Wu, E.L., Kourtzelis, I., Wu, Y.Q., Kaznessis, Y.N., Lambris, J.D., 2011. Novel analogues of the therapeutic complement inhibitor compstatin with significantly improved affinity and potency. Mol. Immunol. 48, 481–489.
Qu, H., Ricklin, D., Lambris, J.D., 2009c. Recent developments in low molecular weight complement inhibitors. Mol. Immunol. 47, 185–195.
Ricklin, D., Hajishengallis, G., Yang, K., Lambris, J.D., 2010. Complement: a key system for immune surveillance and homeostasis. Nat. Immunol. 11, 785–797.
Ricklin, D., Lambris, J.D., 2007. Complement-targeted therapeutics. Nat. Biotechnol. 25, 1265–1275.
Ricklin, D., Lambris, J.D., 2008. Compstatin: a complement inhibitor on its way to clinical application. Adv. Exp. Med. Biol. 632, 273–292.
Roux, S., Zekri, E., Rousseau, B., Paternostre, M., Cintrat, J.C., Fay, N., 2008. Elimination and exchange of trifluoroacetate counter-ion from cationic peptides: a critical evaluation of different approaches. J. Pept. Sci. 14, 354–359.
Sahu, A., Morikis, D., Lambris, J.D., 2003. Compstatin, a peptide inhibitor of complement, exhibits species-specific binding to complement component C3. Mol. Immunol. 39, 557–566.
Sahu, A., Soulika, A.M., Morikis, D., Spruce, L., Moore, W.T., Lambris, J.D., 2000. Binding kinetics, structure–activity relationship, and biotransformation of the complement inhibitor compstatin. J. Immunol. 165, 2491–2499.
Silasi-Mansat, R., Zhu, H., Popescu, N.I., Peer, G., Sfyroera, G., Magotti, P., Ivanciu, L., Lupu, C., Mollnes, T.E., Taylor, F.B., Kinasewitz, G., Lambris, J.D., Lupu, F., 2010. Complement inhibition decreases the procoagulant response and confers organ protection in a baboon model of *Escherichia coli* sepsis. Blood 116, 1002–1010.
Tugyi, R., Uray, K., Ivan, D., Fellinger, E., Perkins, A., Hudecz, F., 2005. Partial D-amino acid substitution: improved enzymatic stability and preserved Ab recognition of a MUC2 epitope peptide. Proc. Natl. Acad. Sci. U. S. A. 102, 413–418.
Wagner, E., Frank, M.M., 2010. Therapeutic potential of complement modulation. Nat. Rev. Drug Discov. 9, 43–56.
Yehoshua, Z., Rosenfeld, P.J., Albini, T.A., 2011. Current clinical trials in dry AMD and the definition of appropriate clinical outcome measures. Semin. Ophthalmol. 26, 167–180.